Electronic structure of fluorinated multiwalled carbon nanotubes studied using x-ray absorption and photoelectron spectroscopy

M. M. Brzhezinskaya,[1,2,*] V. E. Muradyan,[3] N. A. Vinogradov,[2] A. B. Preobrajenski,[4] W. Gudat,[1] and A. S. Vinogradov[2]
[1]*HZB (BESSY), Berlin 12489, Germany*
[2]*St. Petersburg State University, St. Petersburg 198504, Russia*
[3]*Institute of Problems of Chemical Physics, Russian Academy of Sciences, Chernogolovka 142432, Russia*
[4]*MAX-lab, Lund University, S-22100 Lund, Sweden*
(Received 8 January 2009; revised manuscript received 22 February 2009; published 23 April 2009)

This paper presents the results of combined investigation of the chemical bond formation in fluorinated multiwalled carbon nanotubes (MWCNTs) with different fluorine contents (10–55 wt %) and reference compounds (highly oriented pyrolytic graphite crystals and "white" graphite fluoride) using x-ray absorption and photoelectron spectroscopy at C 1*s* and F 1*s* thresholds. Measurements were performed at BESSY II (Berlin, Germany) and MAX-laboratory (Lund, Sweden). The analysis of the soft x-ray absorption and photoelectron spectra points to the formation of covalent chemical bonding between fluorine and carbon atoms in the fluorinated nanotubes. It was established that within the probing depth (~15 nm) of carbon nanotubes, the process of fluorination runs uniformly and does not depend on the fluorine concentration. In this case, fluorine atoms interact with MWCNTs through the covalent attachment of fluorine atoms to graphene layers of the graphite skeleton (phase 1) and this bonding is accompanied by a change in the hybridization of the 2*s* and 2*p* valence electron states of the carbon atom from the trigonal (sp^2) to tetrahedral (sp^3) hybridization and by a large electron transfer between carbon an fluorine atoms. In the MWCNT near-surface region the second fluorine-carbon phase with weak electron transfer is formed; it is located mainly within two or three upper graphene monolayers, and its contribution becomes much poorer as the probing depth of fluorinated multiwalled carbon nanotubes (F-MWCNTs) increases. The defluorination process of F-MWCNTs on thermal annealing has been investigated. The conclusion has been made that F-MWCNT defluorination without destruction of graphene layers is possible.

DOI: 10.1103/PhysRevB.79.155439 PACS number(s): 61.46.Fg, 73.22.−f, 78.70.Dm

I. INTRODUCTION

At present, it was accepted that chemical functionalization of carbon nanotubes (CNTs), i.e., attachment of individual atoms/molecules or their aggregates to CNTs, can extend the field of application of these nanosystems in nanoelectronics, sensorics, hydrogen power engineering, bioengineering, medicine, etc.[1–3] In this respect, the fluorination of CNTs is of special interest because the fluorination results in a considerable decrease in the chemical inertness of the initial systems. Therefore, the fluorination is considered as a promising technological process for the first stage of the CNT chemical functionalization.[4–7] However, carbon materials react with fluorine over a wide range of external conditions. Consequently, the chemical composition, as well as the atomic and electronic structures of fluorinated carbon nanotubes (F-CNTs), depends substantially on the structure and properties of the initial materials and fluorination conditions, such as the reaction temperature and duration, the presence of catalysts, pressure, and concentration of fluorinating reactants.[8] All these factors need comprehensive investigations of fluorination products by different experimental methods.

In spite of great interest in F-CNTs, their atomic and electronic structures have been studied by using a limited number of experimental techniques. First and foremost, these are different microscopic techniques ensuring their visualization,[4–12] x-ray diffraction methods characterizing the degree of F-CNT crystallinity,[9,10] UV spectroscopy,[5] Raman spectroscopy,[4–9,12] and C 1*s* and F 1*s* core-level x-ray photoelectron spectroscopy (XPS),[8,9,12,13] which provide information on the nature of chemical bonding between carbon C and fluorine F atoms in F-CNTs. The investigations performed made it possible to determine the main conditions for the fluorination of single-walled carbon nanotubes (SWCNTs) and multiwalled carbon nanotubes (MWCNTs) to characterize their atomic structure and to obtain preliminary information on the specific features of their electronic structure due to the chemical bonding between C and F atoms. However, the data obtained in those works even with due regard for the results of the first theoretical calculations[14–18] do not provide clear perception of the CNT fluorination mechanism and properties of fluorination products, which is necessary for expansion of practical use of F-CNTs.

Near-edge x-ray absorption fine-structure spectroscopy (NEXAFS) is at present one of the most efficient experimental methods.[19,20] NEXAFS spectroscopy uses the relation between the spectral characteristics of the near-edge fine structure of x-ray absorption spectra and the parameters of the local atomic and electronic structures of the material under investigation in the vicinity of absorbing atoms. There are a few works in which NEXAFS spectroscopy has been successfully used to characterize pristine and oxidized CNTs.[21–27] Total electron yield (TEY) mode is the most popular for recording of NEXAFS spectra.[28,29] At the same time, TEY mode with probing depth approximately equal to the average MWCNT diameter (several tens of monolayers) does not allow one to get information about characteristics of

investigated fluorinated multiwalled carbon nanotubes (F-MWCNTs) in their near-surface region where fluorination process can differ from that at greater depths. However, these data are of genuine fundamental interest and is indeed necessary for optimization of the MWCNT fluorination techniques. Such information for near-surface region only several graphene layers thick can be obtained, particularly, by XPS providing C 1*s* and F 1*s* core-level spectra of F-MWCNTs under investigation. XPS is an effective surface-sensitive method for investigation of material electronic structure.[30] In this case, the probing depth is adequate to the depth the registered electrons are emitted from, which depends on the electron kinetic energy. Therefore, the probing depth can vary from several tenth of nanometer (two to three atomic monolayers) to nanometers, depending on the energy of excitation quanta. Presently, several works with XPS used to characterize fluorinated SWCNTs (F-SWCNT),[7,12,13] fluorinated multiwalled nanoparticles,[31] and F-MWCNTs[32] are known. In the last of these works, core-level photoemission spectra investigation of F-MWCNTs was carried out at only one energy of excitation photons. This energy, 1486.6 eV of the Al K_α x-ray radiation, ensured a little more than 2 nm (approximately six to seven graphene monolayers) probing depth. Based on the spectral parameter analysis of the obtained photoelectron C 1*s* and F 1*s* lines, a conclusion was made that only one fluorine-carbon phase was formed in the probed layer.

The present paper reports on the results of the first investigation of F-MWCNTs with different fluorine contents by x-ray absorption spectroscopy and x-ray photoelectron spectroscopy using synchrotron radiation. The first goal of this study was to understand whether it is possible to use C and F $K(1s)$ x-ray absorption spectra for characterization of the CNT fluorination and to obtain information on the atomic and electronic structures of the functionalization products. It was found out that within the probing depth (~15 nm) of carbon nanotubes, the process of fluorination runs uniformly and does not depend on the fluorine concentration. The second goal of the study was to investigate specific features of F-MWCNTs electronic structure in the near-surface region less than 2 nm thick by varying the excitation energy, and consequently, getting additional information on the process of MWCNTs fluorination. For this purpose, C 1*s* and F 1*s* photoelectron spectra were measured for MWCNTs and F-MWCNTs with various concentrations of fluorine atoms (10–55 wt %) in a wide range of photon energies (1130–385 eV); this ensured the sample probing depth variation in the range of 2–0.4 nm. As a result, existence of two fluorine-carbon phases with chemical bonding characterized by different electron transfer between carbon and fluorine atoms was revealed, and their nature was analyzed. Moreover, it was found out that while one of the phases is located near the surface, the other one is quite uniformly distributed through the probing depth. The third goal of the study was to investigate the MWCNTs defluorination process as exemplified by thermal annealing. Thermal annealing was found to be able to defluorinate F-MWCNTs almost without any destruction of the graphene mesh. Partial information on the research results was reported earlier in Refs. 33 and 34.

II. EXPERIMENTAL DETAILS

MWCNTs were produced by arc-discharge evaporation of graphite rods (extremely pure, spectral purity, 99.9992 wt %) in the helium atmosphere (500 Torr) at current density of 175 A/cm^2 and voltage of 23 V.[35] Material with multiwall nanotubes was withdraw from the cathodic deposit center and had a columnar structure with the column length of up to 10 mm (see, e.g., Ref. 36).

The carbon-based material containing nanotubes was only grinded and screened by using a sieve with 0.25 mm mesh without any chemical treatment. High-resolution transmission electron microscope (HRTEM) images of initial material clearly demonstrate the laminar structure of multiwall nanotubes with always open nanotubes ends, which is characteristic of similar products synthesized by other researchers by the arc-discharge method.

The powdered samples of MWCNTs were fluorinated in a nickel reactor at the temperature T_F=420 °C in a flow of molecular fluorine produced by electrolyzing acidic potassium trifluoride KF·2HF containing up to 3 wt % of HF. The chemical analysis for the fluorine content in the samples was carried out by preliminarily burning the fluorinated material with Na_2O_2 in order to transform fluorine into a water-soluble form, followed by the titration of F^- ions with thorium nitrate.

Powdered "white" graphite fluoride (WGF) was prepared as follows. A coke was purified using the industrial thermochemical method at a temperature of 2800 °C. The impurity content was less than 10^{-4} wt %. Then, the coke was fluorinated according to the procedure similar for the MWCNTs at T_F=300 °C. The product with a maximum fluorine content of 62.4 wt % was almost white in color. A highly oriented pyrolytic graphite (HOPG) crystal (degree of perfection, Grade SPI-1) was purchased from SPI Supplies. In this work, the spectra of WGF and HOPG were used as the reference spectra.

The C 1*s* and F 1*s* x-ray absorption spectra of the pristine and fluorinated MWCNTs, HOPG, and WGF were measured using monochromatic synchrotron radiation and the facilities of the Russian-German beamline (RGBL) at the BESSY II (Berlin).[37] The samples for x-ray absorption and photoelectron measurements were prepared in air. The powders of the MWCNTs and WGF were rubbed into a scratched surface of a pure substrate (metallic indium plate 7×7 mm^2 in size) in order to ensure the substrate uniform surface coating without any noticeable gaps. For other details of sample preparation see Ref. 33.

The NEXAFS spectra were obtained by recording the TEY of the x-ray photoemission[28,29] in the mode of measurement of the drain current of the sample by varying the energy of incident photons. No noticeable charging of the sample irradiated by a high-intensity beam of monochromatic synchrotron radiation in the ultrasoft x-ray range was observed in the course of measurements. All x-ray absorption and photoelectron spectra were measured under ultrahigh vacuum ($\sim2\times10^{-10}$ Torr). The sample was adjusted to the synchrotron-radiation beam with the use of visible light reflected from the diffraction grating of the monochromator in the 0th diffraction order. The samples were located at an

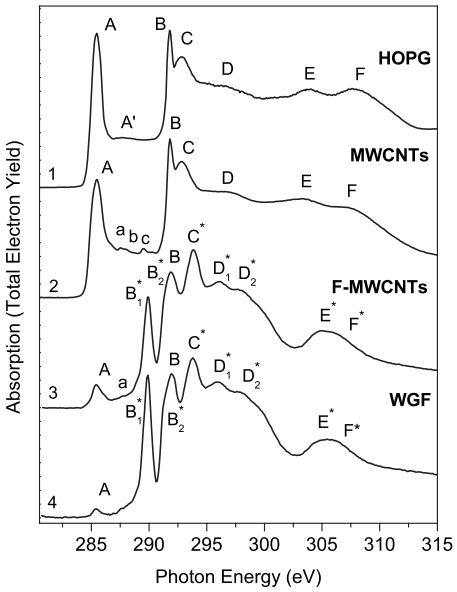

FIG. 1. Near-edge fine structure of the C 1*s* absorption spectra of (1) the HOPG, (2) pristine MWCNTs, (3) MWCNTs+F55%, and (4) WGF (C_F=62.4%). The spectra are normalized to the intensity of continuous absorption at the photon energy of 315 eV.

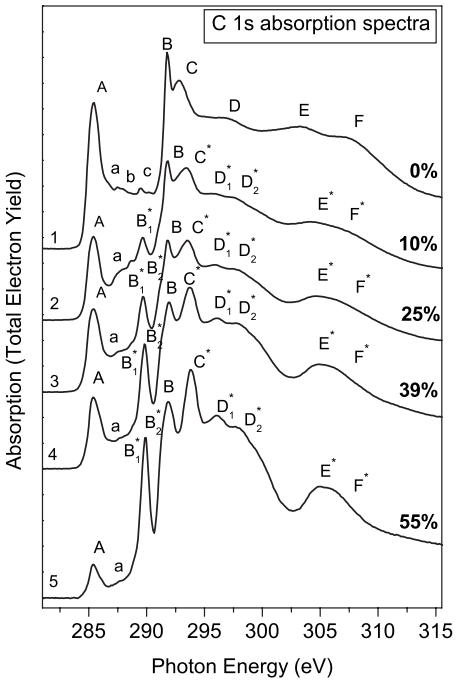

FIG. 2. C 1*s* absorption spectra of (1) the pristine MWCNTs and (2–6) F-MWCNTs containing (2) 5%, (3) 10%, (4) 25%, (5) 39%, and (6) 55%. All the spectra are normalized to the intensity of continuous absorption at photon energy of 315 eV.

angle of ~45° with respect to the incident beam of monochromatic radiation. The size of the focused spot on the sample was $\sim 0.2 \times 0.1$ mm^2.

The energy resolutions ΔE of the monochromator in the range of the F 1*s* x-ray absorption edge (photon energy $h\nu \sim 680$ eV) and the C 1*s* x-ray absorption edge ($h\nu \sim 285$ eV) were equal to ~150 and 70 meV, respectively. The x-ray absorption spectra were normalized with respect to the incident photon flux, which was monitored by recording the TEY from the clean surface of a gold crystal mounted on the manipulator holder. The $h\nu$ in the range of the fine structure of the F and C x-ray absorption spectra was calibrated against the energy positions of the first narrow peak in the F 1*s* x-ray absorption spectrum of K_2TiF_6 [683.9 eV (Ref. 38)] and the C 1*s* x-ray absorption spectrum of HOPG [285.45 eV (Ref. 39)]. The F 1*s* and C 1*s* core-level photoelectron spectra necessary for comparing the measured x-ray absorption spectra of F-MWCNTs on the same energy scale were recorded at $h\nu$=1030 eV.

In recording x-ray photoelectron spectra, $h\nu$ varied from 345 to 1130 eV. Energy resolution ΔE of the monochromator with the 200 μm exit slit was 145–750 meV within the above mentioned range of $h\nu$. Photoelectron spectra of all the samples were measured in the normal photoemission registration mode by using the Phoibos 150 spherical analyzer from Specs whose resolution in recording the spectra remained equal to 200 meV. The analyzer was calibrated against energy based on photoelectron spectra of Au atom $4f_{7/2,5/2}$ electrons. The monochromator was calibrated by recording the basic photoelectron lines of C 1*s* spectra exited by radiation reflected from the diffraction grating in the first and second diffraction orders.

To control compositions of the samples, general photoelectron spectra at $h\nu$=1030 eV within the bounding energy (BE) range of BE=0–900 eV were measured for all of them. They showed the presence of a small amount of oxygen (<1%) in the samples, which can be partly explained by the presence of oxide on the In substrate used in the experiments.

Several samples of each type were prepared; spectra of each sample were measured with good statistics at several different points of a sample. In addition, many of the absorption and photoelectron measurements were repeated at MAX-laboratory by using the D1011 beamline equipment[40] having almost the same spectral characteristics as RGBL. In repeating the measurements, we observed only insignificant variations in relative intensities of spectrum features; this is the evidence of good reproducibility of measurements and high homogeneity of initial and fluorinated MWCNT powders.

The defluorination experiments were carried out at the D1011 beamline in MAX-laboratory (Lund, Sweden). Copper foil was used as a substrate. Temperature was controlled by a thermocouple secured on a special holder just next to the sample. The electron structure variations in the samples were monitored by using NEXAFS spectroscopy in the sample drain current recording mode.

III. EXPERIMENTAL RESULTS AND DISCUSSION

A. NEXAFS spectra

The measured C $K(1s)$ and F $K(1s)$ x-ray absorption spectra of the pristine and fluorinated MWCNTs, the HOPG, and WGF are depicted in Figs. 1–4. It should be noted that the x-ray absorption spectra of F-MWCNTs prepared with

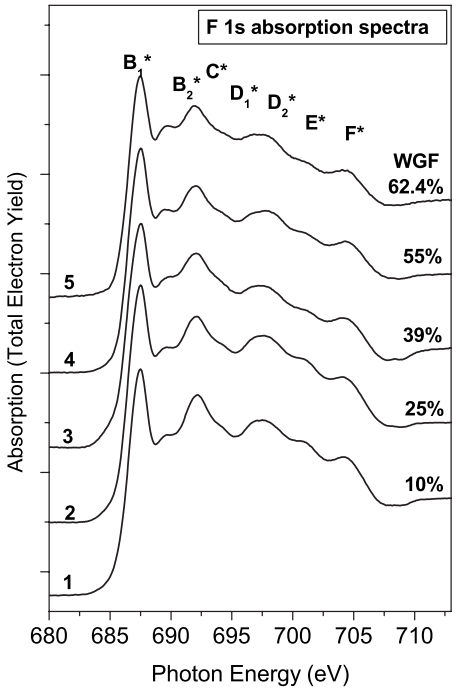

FIG. 3. Near-edge fine structures of the F 1*s* absorption spectra of WGF (6) and (1–5) F-MWCNTs containing (1) 5%, (2) 10%, (3) 25%, (4) 39%, and (5) 55%. All the spectra are normalized to the intensity of continuous absorption at the photon energy of 715 eV.

the use of different conditions or fluorination techniques have never been investigated.

The spectrum of HOPG (Fig. 1, curve 1) is in good agreement with the results of previous measurements performed with a similar high-energy resolution (~100 meV).[23,39,41] It is also known that the most characteristic absorption peaks (resonances) *A* and *B*-*C* in the HOPG spectrum are associated with the dipole-allowed transitions of the 1*s* electrons of

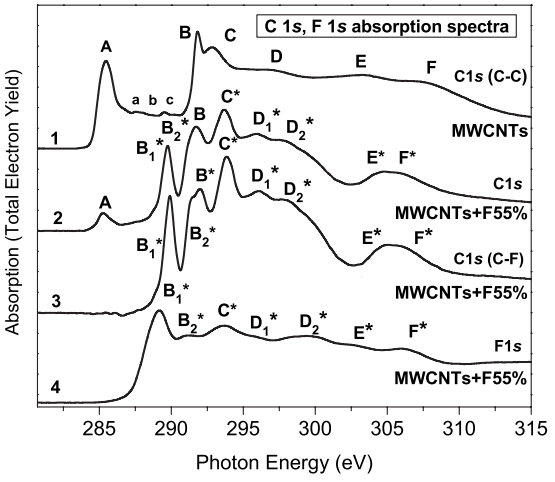

FIG. 4. Comparison of F 1*s* NEXAFS and two components of C 1*s* NEXAFS spectra of MWCNTs+F55%. The F 1*s* absorption spectrum is reduced to the energy scale of the C 1*s* absorption spectrum with the use of energy spacing ΔE(F 1*s*-C 1*s*) =398.4 eV (measured by x-ray photoemission spectroscopy) between the F 1*s* and C 1*s* core levels.

the carbon atom to the free π and σ states in the conduction band of the HOPG. These states are formed by the C $\pi 2p_z$ and C $\sigma 2p_{x,y}$ states oriented perpendicular and parallel to the plane of the carbon layer (graphene), respectively. These states are quasimolecular in nature, i.e., they are similar to the free-electron states in the molecule of benzene C_6H_6.[42] Therefore, these states are predominantly localized within one carbon hexagon and manifest themselves in the form of discrete transitions in the spectrum of the HOPG. The very broad band A' responsible for a considerable absorption intensity between the resonances *A* and *B* also reflects the electronic transitions to the free π states, which are more delocalized in the graphene layer. The bands *D*–*F* are attributed to the electronic transitions to the free σ states in the conduction band of graphite, which are associated with the interaction of carbon hexagons in the graphene layer.

The C 1*s* x-ray absorption spectrum of the pristine MWCNTs (curve 2) is very similar to the C 1*s* spectrum of the HOPG (curve 1). This similarity suggests a high quality of the atomic structure of the synthesized MWCNTs and the absence of a noticeable contribution from amorphous and other possible phases. However, there are some insignificant differences in the spectrum of the MWCNTs: the features *a*, *b*, and *c* between the absorption bands *A* and *B*-*C* and a small broadening of all structural features. The band *A* full width at half maximum (FWHM) height increases from 1.15 for HOPG to 1.45 eV for MWCNTs. This broadening is attributed to the splitting of the $\pi 2p_z$ conduction subband of graphite due to the bending of graphene layers and their symmetry reduction in the MWCNTs. The appearance of the features *a*, *b*, and *c* is associated with the transitions of the C 1*s* electrons to the free 2*p* states in surface nanotube regions oxidized during the synthesis.[21,24] The existence of small amounts (<1 wt %) of chemically bound oxygen in the MWCNTs is confirmed by mass spectrometric analysis of the gas products released from the MWCNTs upon their heating[43] and the results of our x-ray photoelectron measurements (see Sec. III B).

What is most important is that the C 1*s* NEXAFS spectra of the F-MWCNTs with the highest fluorine content (C_F=55 wt %) (MWCNTs+F55%) and WGF (Fig. 1, curves 3 and 4) are very similar and differ substantially from the spectra of HOPG and MWCNTs (Fig. 1, curves 1 and 2). The most significant differences involve a drastic decrease in the intensity of the resonance *A* and the band A' associated with the free π states and the appearance of the high-energy σ band E^*-F^*. It is evident that the observed changes are governed by the fluorination of the HOPG and MWCNTs. The resonance *A* is retained in the spectra of the fluorinated samples but has a considerably lower intensity with respect to the other spectral portion associated with the transitions of the 1*s* electrons to the free σ states of the conduction band. The band *B* is also retained in the spectra, whereas the other specific features in the spectra of HOPG and MWCNTs have no clear analogs in the spectra of the fluorinated samples. New specific features B_1^*-F^* in the spectra of the F-MWCNTs and WGF should be unambiguously treated as a result of the transitions of the C 1*s* electrons to the free states of the new phase formed in the MWCNTs and HOPG due to their fluorination. It should be emphasized

that in the given case, only one particular phase can be formed. In the presence of several fluorocarbon phases, the C 1*s* spectra would be virtually structureless and similar in this respect to the spectrum of amorphous carbon.[44] Hence, the spectra of the F-MWCNTs and WGF are a superposition of the dominant C 1*s* spectrum of the fluorocarbon phase and the low-intensity spectrum of the pristine sample (MWCNTs and HOPG). In other words, despite the maximum possible fluorine content in the F-MWCNTs and WGF (55.0 and 62.4 wt %, respectively), they are incompletely fluorinated and contain regions composed of the pristine HOPG and MWCNTs. This is most probably explained by the fact that a limiting depth of fluorination exists under these conditions of the synthesis. This fluorination depth is less than the probing depth ($d \sim 15$ nm) of the sample when the TEY method is employed for recording the NEXAFS spectra.[19,20] Since the sample contains MWCNTs of different sizes ($L \sim 0.5-2.0$ μm and $D \sim 10-30$ nm), including nanotubes with a diameter $D > 15$ nm, the measured C 1*s* spectrum should involve the contributions of the fluorinated and pristine carbon phases.

Since the C 1*s* NEXAFS spectra of the F-MWCNTs and WGF do not contain the intense π resonance *A* and the π band *A'*, we can make the inference that the C atoms are involved in the chemical bonding upon formation of the fluorocarbon phase. This implies that upon fluorination, the F atoms are attached to the graphene layer perpendicular to it rather than replace the C atoms in the layer. In this case, the F atoms form bonds with the C atoms with the participation of the C $2p_z$ states. As a result, the C atom has a spatial coordination rather than the planar coordination. The above inference is confirmed by a direct comparison of the C 1*s* NEXAFS spectrum of the fluorocarbon phase with the spectra of molecules of fluorobenzenes $C_6H_{6-n}F_n$ ($n=1-6$),[45] in which the planar coordination of carbon atoms is retained. Actually, the compared spectra differ substantially and the π resonances are observed in the spectra of all fluorobenzenes.

One more indirect evidence for the change in the coordination of the C atom in HOPG and MWCNTs during fluorination can be the appearance of a single σ band E^*-F^* in the x-ray absorption spectra of the fluorinated samples ($h\nu \sim 303-310$ eV). A similar high-energy band, together with the absence of the π resonance, is considered as a characteristic difference between the C 1*s* NEXAFS spectrum of diamond with the sp^3 tetrahedral coordination of the C atoms and the spectrum of HOPG with the sp^2 trigonal coordination.[42] This conclusion is in good agreement with the results obtained from the investigation into the mechanism of the formation of graphite fluoride C_xF by Raman spectroscopy.[46]

In this respect, it is interesting to compare the C 1*s* x-ray absorption spectra of the F-MWCNTs with different fluorine contents (0%–55%) (Fig. 2) because they correspond to different stages of the MWCNT fluorination. These spectra demonstrate a monotonic character of variations in the fine structure with an increase in the degree of MWCNT fluorination. As a result, a gradual disappearance of the π structure (the resonance *A* and the band *A'*), as well as the formation of the characteristic resonances and in the region of the σ structure in addition to a single high-energy band E^*-F^*, is observed. These changes manifest the uniform character of the interaction between the F and C atoms in all stages of the fluorination process.

The above conclusion is confirmed by the results of comparison of the F 1*s* x-ray absorption spectra of F-MWCNTs (Fig. 3). All the F 1*s* x-ray absorption spectra of the F-MWCNTs and WGF exhibit a similar fine structure. The main difference between the spectra is that the measured intensity of the spectra increases monotonically with respect to the background intensity with increasing fluorine content in the F-MWCNTs. This behavior of the F 1*s* x-ray absorption spectra of the F-MWCNTs with an increase in the fluorine content in the samples can be interpreted only as a result of the formation of a fluorocarbon phase, which is identical in all stages of the fluorination process. This conclusion, of course, should correlate with the probing depth (~15 nm) of the nanotube samples during the recording of the x-ray absorption spectra in this work.[19,20]

The F 1*s* x-ray absorption spectra are also characterized by rich and clearly pronounced fine structure. This circumstance indicates a well-defined atomic structural order in the fluorinated samples. In other words, the fluorine atoms, such as the carbon atoms, have an identical coordination, which reflects chemical bonding of the C and F atoms.

For the characterization of the spectrum of free-electron states in fluorinated samples, the C 1*s* x-ray absorption spectrum is compared in Fig. 4 with the F 1*s* spectrum of MWCNTs+F55%. These spectra are made coincident in energy by reducing the F 1*s* spectrum to the energy scale of the C 1*s* spectrum with the use of the energy spacing ΔE(F 1*s*-C 1*s*)=398.4 eV between the F 1*s* and C 1*s* core levels. The C 1*s* NEXAFS spectrum of F-MWCNTs can be decomposed into two components corresponding to the electron transition from the 1*s* core level of the carbon atoms bonded only to carbon atoms and of those bonded to the fluorine atoms using the NEXAFS spectrum of the pristine MWCNTs as a reference. By comparing the absorption fine structures in these spectra, one can see that the component corresponding to the C-F bonded atoms has nearly the same fine structure as the F 1*s* spectrum (details B_1^*-F^*). The characteristic for the C-F bond peaks B_1^* and C^* are of near-equal energy positions in F 1*s* spectrum and in C 1*s* spectrum of carbon atoms bonded to fluorine atoms. The corresponding fine structure is absent in the C 1*s* spectrum of the C atoms bonded to other carbon atoms. The energy misalignment of peaks B_1^* can be explained by the different strength of the core hole potential at carbon and fluorine sites. This finding gives additional evidence for a covalent bonding between the carbon and fluorine atoms in F-MWCNTs. This inference is in complete agreement with the conclusion regarding the sp^3 hybridization of the valence electron states of the carbon atoms, which was drawn previously from a separate analysis of the absorption spectra of carbon and fluorine. This conclusion is also supported by the fact that the spectra of fluorine do not exhibit an analog of the π resonance *A*, which is observed in the C 1*s* x-ray absorption spectra of the initial materials (HOPG and MWCNTs).

Notice that the above-made conclusion on the covalent character of fluorine-carbon bonds in F-MWCNTs and retention of laminar character of the carbon atomic structure up to

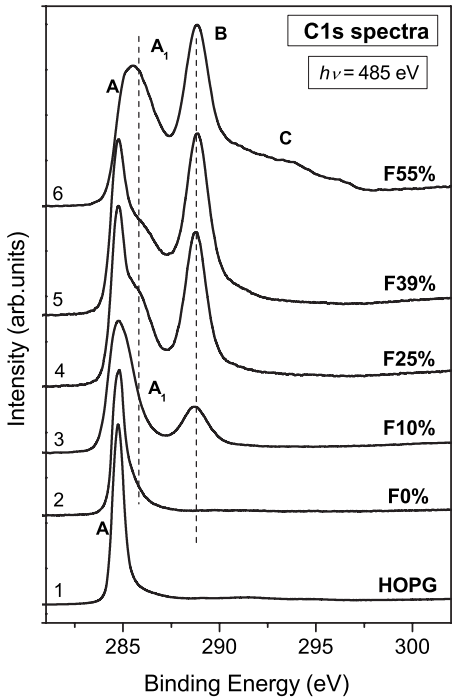

FIG. 5. C 1*s* x-ray photoelectron spectra of HOPG (1), pristine (2), and F-MWCNTs with different fluorine concentrations, 10% (3), 25% (4), 39% (5), and 55% (6), measured at the photon energy of 485 eV.

maximal fluorine concentrations ensuring the binary (CF) stoichiometry of fluorination products agrees well with well-known results of graphite fluorination. It was found out for graphite that when it is maximally fluorinated, fluorine-carbon phase poly(carbon monofluoride) $(CF)_n$ predominates,[46,47] which is characterized by the retention of laminar graphitelike structure, although the layers are no longer planar but become corrugated because fluorine atoms are attached to them. What is important is that this graphite fluoride is characterized by covalent binding with sp^3 hybridization of carbon-atom valent states. This fact is confirmed also by the similarity of absorption spectra of F-MWCNTs and WGF reference samples. All this confirms the above conclusion that MWCNTs retain their basic structure at high fluorination levels, such as 55 wt %, where almost every carbon atom throughout all CNT layers is in the sp^3 configuration.

B. XPS spectra

X-ray photoelectron spectra for HOPG, MWCNTs, and F-MWCNTs were measured using 345–1130 eV excitation photons. Figure 5 shows x-ray photoelectron C 1*s* spectra ($h\nu$=485 eV and total-energy resolution of ~220 meV). The HOPG spectrum is a single C 1*s* line accompanied on the higher BE side by a satellite structure consisting of three quite narrow lines (see Fig. 6) and the fourth broad band, which are 4.4, 6.7, 10.1, and ~27 eV apart the major peak, respectively. The HOPG C 1*s* spectrum main line is a narrow peak at BE=284.8 eV having asymmetric shape on the higher bounding energy side and FWHM of 0.6 eV.

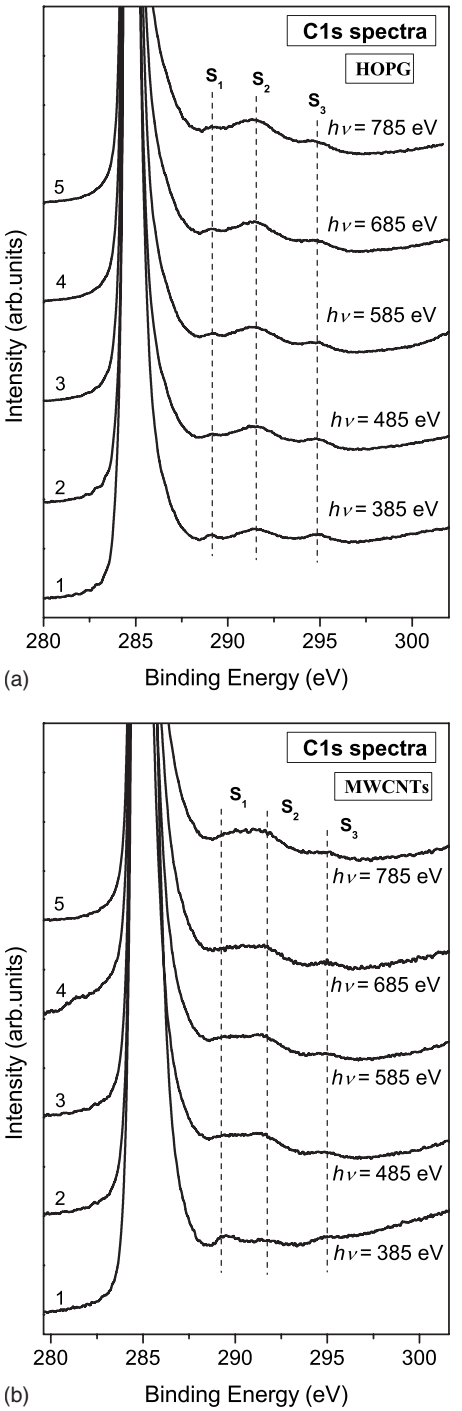

FIG. 6. Satellites structures near the C 1*s* peak in the x-ray photoelectron spectra of (a) HOPG and (b) pristine MWCNTs.

The C 1*s* photoelectron line of initial MWCNTs is located at the same energy BE=284.8 eV as that of HOPG, but its shape is more asymmetric on the higher-energy side. The main peak in MWCNTs XPS C 1*s* spectrum, as well as that in HOPG spectrum, is accompanied by four satellites whose positions with respect to the C 1*s* peak [4.6, 6.6, 10.1 eV (see Fig. 6), and ~26.5 eV] are almost the same as in the HOPG spectrum. It allows us to assume that the satellites in MWCNTs and HOPG spectra are of the same origin and are associated with discrete energy losses of emitted C 1*s* pho-

toelectrons for valence electron excitation in the graphene layer (shake up, inelastic scattering, and plasmon excitations).[30] The energy gap between the second satellite and the main C 1*s* line is close to the energy of the known CNT π plasmon that is observed in the processes of characteristic electron energy losses.[48] Therefore, the presence of this satellite can be regarded as a result of C 1*s* photoelectron energy losses for excitation of valence π-electron collective oscillations.

The satellite structure discreetness of HOPG [Fig. 6(a)] is markedly weaker than that of MWCNTs [Fig. 6(b)]. This effect is clearly seen while comparing the MWCNTs and HOPG spectra measured at all photon energies in the $h\nu$ =345–1130 eV range. Moreover, the first three satellites are distinctly seen only for $h\nu$=345–685 eV provided that their energy positions in the MWCNTs C 1*s* photoelectron spectrum remain the same, while for higher-energy photons the first satellite gets blurred against the background of the second one that, together with the third satellite, is observed without energy shift up to $h\nu$=1130 eV. The last fact cannot be explained by the loss of total resolution due to the decrease in the monochromator resolution (from 405 to 860 meV as the photon energy changes from $h\nu$=685 eV to $h\nu$ =1130 eV) because nothing of that kind has been observed in respective HOPG spectra obtained under the same experimental conditions. Therefore, it is possible to connect the observed loss in the discreetness of the nanotubes spectrum satellite structures with the broadening of satellite lines and changes in their relative intensity, which seem to be due to some small differences in electronic structures of flat and rolled graphene layers.

C 1*s* photoelectron spectrum structure changes radically as initial MWCNTs are transformed into F-MWCNTs (Fig. 5). Shoulder A_1 shows up near the main line *A* at BE =285.7 eV, and the second line *B* arises at BE=288.8 eV. While the fluorine concentration in F-MWCNTs grows, the intensities of the new features increase, while their energy positions do not change. When the concentration reaches C_F=39 wt %, intensity *B* becomes almost equal to the main C 1*s* line intensity *A*. Spectrum measured at the maximum fluorine concentration (C_F=55 wt %) differs significantly from the other spectra; band *A* almost fully disappears against the background of the intense band into which shoulder *A* is transformed, whereas band *B* becomes the most intense structure feature having an intense, extended, and poorly structured tail *C* on the high-energy side.

As shown above, emergence of new features in the MWCNTs+F39% C 1*s* spectrum structure as compared with those of MWCNTs can be attributed to CNTs fluorination; therefore, it can be regarded as a result of carbon-to-fluorine chemical bonding. This interaction results in formation of fluorine-carbon phases and is accompanied by charge transfer from carbon atoms to fluorine atoms due to the fact that fluorine electronegativity is higher. Charge states (oxidation rates) of carbon atoms in at least two of the fluorine-carbon phases are different and can be characterized by chemical shifts of their C 1*s* photoelectron lines (peaks A_1 and *B*) from the energy position of this line in pristine MWCNTs spectrum (peak *A*). Energy positions of bands A_1 and *B* relative to peak *A* are significantly different (0.9 and 4.0 eV, respectively). This large difference (>3 eV) indicates considerable differences in the natures of C-F atom interactions in the analyzed fluorine-carbon phases that are formed in F-MWCNTs.

The first fluorine-carbon phase (phase 1, peak *B*) is characterized by the most intense electron-density transfer from carbon atoms to fluorine atoms. Evidently, this phase arise due to covalent attachment of fluorine atoms to the graphene layer. Below it is shown that contrary to the second (near-surface) phase associated with peak A_1, this phase does not disappear with increasing probing depth. Therefore, it can be reasonably assumed to be the unique fluorocarbon phase that we have observed in the MWCNTs C 1*s* absorption spectra in deeper probing.[33] In this case, fluorine atoms do not substitute for carbon atoms in the graphene layer but get attached to it perpendicularly via $2p_z$ states of the carbon atom, and thus, preparing for the latter spatial (sp^3) coordination with additional σ(F $2p$-C $2s,2p_z$) bonding instead of planar (sp^2) coordination. The idea that photoelectron signal *B* and fluorocarbon phase that was observed in absorption spectra earlier[33] is consistent with the fact that chemical shifts observed in photoelectron and absorption C 1*s* spectra of F-MWCNTs are close to each other: 4.0 and 4.45 eV, respectively.

C 1*s*-electron BE chemical shift for phase 2 (0.9 eV) is much smaller than that for phase 1 (4.0 eV). It means that formation of the second fluorocarbon phase is accompanied by a significantly weaker electron-density transfer from carbon-to-fluorine atoms, and consequently, has a weaker chemical bond. Obviously, the difference in carbon-atom chemical states in the fluorocarbon phases under consideration should manifest itself in the difference in their spatial structures, particularly, in the growth of interatomic C-F distances in transition from phase 1 to phase 2.

The most important difference between the MWCNTs +F55% C 1*s*-electron spectrum and spectra of nanotubes with lower fluorine content is low band *A* intensity (C 1*s* signal from initial MWCNTs) as compared with A_1 and *B* band intensities (C 1*s*-photoelectron lines for the two fluorocarbon phases) and feature *C*. The first fact demonstrates that when the fluorine concentration in the subsurface region of about 0.6 nm thick, which is probed at $h\nu$=485 eV, is maximal, the number of carbon atoms not bounded to fluorine atoms is significantly smaller than the number of atoms bounded with fluorine.

Feature *C* indicates that a great number of electrons emerging in MWCNTs+F55% have higher oxidation rates compared to C atom oxidation rates in phases 1 and 2. In this case, C atom chemical states are characterized by even greater electron-density transfer from carbon atoms to fluorine ones because the feature *C* chemical shift is notably larger (6–11 eV) than that of peak *B* (4 eV). Such large chemical shifts have been already known for fluoromethanes $CH_{4-n}F_n$ (n=0–4) whose C 1*s*-electron bounding energies increase by 11 eV with the increase in the number of fluorine atoms in the molecule.[20] Comparing the F-MWCNTs and $CH_{4-n}F_n$ spectra, we can assume that the existence of carbon atoms with high oxidation rates in MWCNTs+F55% probed regions is associated with formation of various fluorocarbon clusters C_mF_n ($n>m$) in the process of fluorination. Empha-

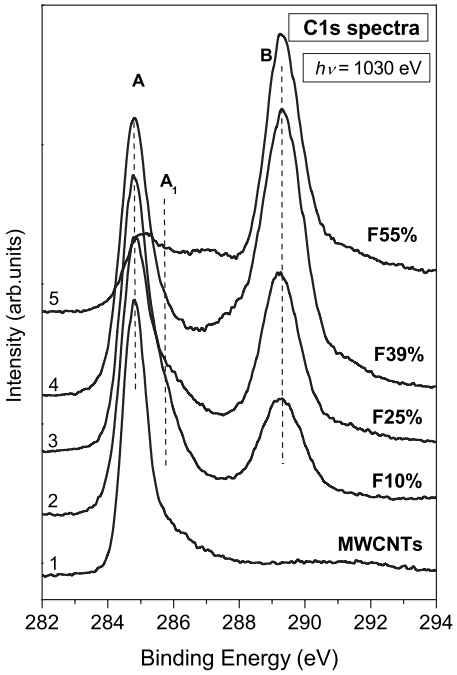

FIG. 7. C 1*s* x-ray photoelectron spectra of pristine (1) and fluorinated MWCNTs with different fluorine concentrations, 10% (2), 15% (3), 25% (4), 39% (5), and 55% (6), measured at the photon energy of 1030 eV.

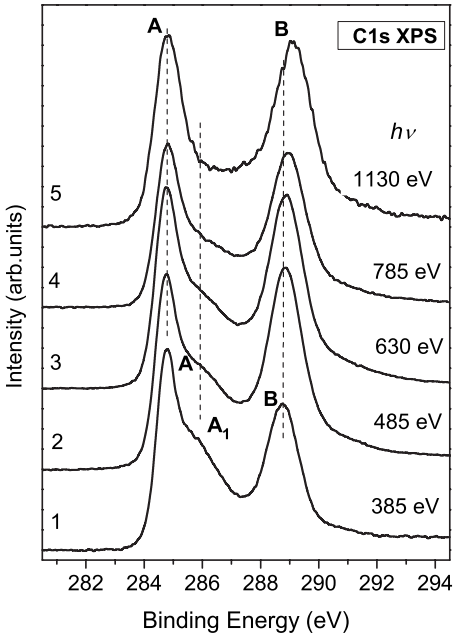

FIG. 8. C 1*s* x-ray photoelectron spectra of MWCNTs+F39% measured at photon energies of 345 eV (1), 630 eV (2), 730 eV (3), and 1030 eV (4).

size that contrary to the above-discussed fluorocarbon structures, those clusters, due to the fact that their carbon atoms are in different chemical states, cannot form a united structurally ordered phase, and therefore, produce a quasiamorphous formation. So we can talk about the outer layers of nanotubes starting to turn into amorphous state in the MWCNTs+F55% sample.

Let us compare C 1*s*-photoelectron spectra obtained at $h\nu$=485 eV and $h\nu$=1030 eV ($d\sim 2$ nm) (Fig. 7). Relative intensities of bands *A* and *B* do not change much with $h\nu$ increasing up to 1030 eV, while the A_1 band intensity decreases, and the corresponding shoulder gets barely visible against band *A* background.

It is reasonable to connect those observations with the probing depth increase from ~0.6 nm (one to two graphene layers) to 2 nm (five to six layers). The weak relationship between the peaks *A* and *B* relative intensities indicates that the ratio of the initial and fluorinated MWCNTs phases for the samples with C_F=10–39 wt % changes only slightly with depth within several graphene layers. This statement is consistent with the conclusion made earlier in Sec. III A and in Ref. 33; that conclusion states that the fluorination process in MWCNTs under investigation remains uniform within the depth limits of ~15 nm.

A significant decrease in the band A_1 intensity with the probing depth increase from 0.6 to 2 nm shows unambiguously that phase 2 is of the near-surface character and is formed by fluorination of only a few outer graphene layers. This conclusion is consistent with the specific shape of C 1*s* photoelectron spectrum obtained for MWCNTs+F55%. Figure 7 shows that a significant decline of band *A* (initial MWCNTs signal) as compared with band *B* (spatial fluorocarbon phase signal), which is similar to that observed at $h\nu$=485 eV, is not accompanied by an increase in the band A_1 intensity. For MWCNTs+F55% spectra, the intensity of feature *C* also decreases with decreasing probing depth. It means that the above mentioned quasiamorphization of nanotubes occurs only in the near-surface layer of maximally fluorinated MWCNTs.

The energy gap between bands *A* and *B* grows by ~0.5 eV as photon energy changes from $h\nu$=485 eV to $h\nu$=1030 eV. It means that chemical shift of the C 1*s* level grows from 4.0 to 4.5 eV with increasing probing depth for spatial fluorocarbon phase. Such an increase in the chemical shift is observed for $h\nu>700$ eV only (see below). It may be a result of a small change in the chemical state of phase 1 carbon atoms located deeper in the samples. In this case, the chemical shift of 4.5 eV for C 1*s* level is practically equal to the 4.45 eV chemical shift in the C 1*s* absorption spectra[35] and, within the experimental accuracy, is equal to the chemical shift of 4.7–4.8 eV detected earlier for similar samples ($h\nu$=1486.6 eV).[32]

The feature A_1 behavior is similar in all F-MWCNTs spectra; Fig. 8 represents MWCNT+F39% to illustrate this fact. The band A_1 intensity gradually decreases with increasing probing depth (d=0.4–2 nm and $h\nu$=345–1130 eV). The band A_1 transformation cannot be caused by its blurring, resulting from the total drop of the energy resolution as $h\nu$ is increasing. Hence, it is reasonable to connect the gradual band A_1 weakening with formation of fluorocarbon phase in the very near-surface layer of the tubes. This layer is one to two graphene monolayers thick as this is just the depth (0.4–0.8 nm), where from C 1*s* photoelectrons generated by absorption of quanta with $h\nu$=345–630 eV and having kinetic energies of E_k=60–345 eV can be emitted without energy losses.[30,49,50]

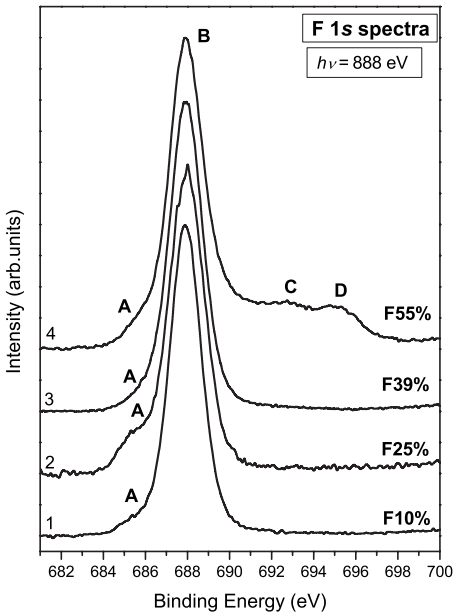

FIG. 9. F 1*s* x-ray photoelectron spectra of F-MWCNTs with different fluorine concentrations, 10% (1), 25% (2), 39% (3), and 55% (4) measured at the photon energy of 888 eV.

In addition, F 1*s* spectra with $h\nu$=788–1088 eV were also measured for F-MWCNTs. The photoelectron kinetic energies were here about $E_k \sim 100-400$ eV, which corresponds to the probing depth of about $d \sim 0.5-1.0$ nm.[30,50] F 1*s* photoelectron spectra ($h\nu$=888 eV) (Fig. 9) consist of the main peak *B* and shoulder *A* that is 2 eV apart the main peak. There is also a high-energy satellite shaped as a broad band, which is about 32 eV apart the main peak (not shown in the figure). For F-MWCNTs, the structural details of F 1*s*-photoelectron spectra keep their energy positions and, contrary to the C 1*s* spectra, do not exhibit any significant changes in their shapes up to C_F=39 wt %. This regularity is also true for F 1*s* spectra measured at other $h\nu$ (788–1088 eV) and was observed earlier at quanta with higher energies ($h\nu$=1486.6 eV).[32]

The absence of any significant relationship between the F 1*s* photoelectron spectrum structure and fluorine concentration in nanotubes can be explained as follows. The F 1*s* spectra are less informative as compared to the C 1*s* spectra. The effective charge of fluorine atom in F-MWCNTs, as in the most of other compounds, is negative and varies in a limited range from 0 to −1 when the atom chemical state changes. A small change in the valence electron density in a fluorine atom is accompanied, due to its participation in chemical bonding with carbon atoms, by a weak change in screening of F 1*s* core-level electrons by valence electrons, which manifests itself in small values of chemical shifts of F 1*s* electron bounding energies. For example, for fluorobenzene molecules, $C_6H_{6-n}F_n$ (n=1–6), BE of F 1*s* electrons grows by 0.2–0.3 eV for each fluorine atom added successively to carbon hexagon.[49] As a result, chemical shift of the F 1*s* peak, in case C_6H_5F transforms to C_6F_6, is 1.3 eV only, which is considerably lower than the ~4 eV chemical shift observed for C 1*s* electrons. Small chemical shifts of F 1*s* peaks and FWHM ~2.3 eV that are significantly higher than the FWHM of C 1*s* peaks (~1.3 eV) restrict severely the possibility of F 1*s* photoelectron spectra analysis to be used in characterizing the chemical states of fluorine atoms in fluorocarbon structures of F-MWCNTs.

Since at $h\nu$=888 eV the probing depth is very small, $d \leq 0.6$ nm, the fluorine spectrum should comprise, together with the main peak *B* originated from F 1*s* electrons involved in covalent bonds with carbon atoms, an additional less intensive structure caused by a weaker bonded fluorocarbon compound existing in the near-surface layer of F-MWCNTs. According to the C 1*s* spectra analysis, this structure should be similar to the A_1 shoulder on the C 1*s* spectra (Fig. 5). For this near-surface compound, the electron transfer between carbon and fluorine atoms is substantially weaker than that for the covalent compound, and consequently, the negative charge of fluorine atoms is substantially smaller. Hence, structure A_1 should be located at larger BE than the main peak *B*. However, F 1*s* spectra of F-MWCNTs with $C_F < 55\%$ (Fig. 9) do not contain pronounced indications of such a feature.

C. Results of defluorination experiments

Changes in MWCNT structure caused by its fluorination were discussed earlier in Secs. III A and III B. On the other hand, investigation of CNT defluorination process can contribute to getting some additional data on the nature of those changes, i.e., make it possible to estimate the type and power of carbon-fluorine bonding and to find out whether the graphene mesh is distorted. Thermal annealing is one of the possible methods of F-CNT defluorination. This paper illustrates thermal annealing as exemplified by an MWCNTs +F39% sample. As noticed above, the sample position with respect to incident radiation did not change during the experiment, which made it impossible to get data from different sites on the surface. The annealing started at the temperatures much lower than the fluorination one, T_F. After the first three annealing stages at T_{DF}=200, 320, 350 °C (t=15 min each), no changes were revealed in C 1*s* and F 1*s* absorption spectra [Figs. 10(a) and 10(b), curve 2]. Such results testify to the absence of changes in the F-MWCNTs atomic structure in the probed region. The first changes in the C 1*s* absorption spectrum structure were observed only after the fourth annealing carried out during 15 min as well but at the temperature close to T_F of initial MWCNTs (T_{DF}=400 °C). The changes manifested themselves in small reduction in bands B_1^* and D_1^*, D_2^* relative intensities and growth of the bands *A* and *B* intensities [Fig. 10(a), curve 3]. Bands B_1^* and D_1^*, D_2^* in the C 1*s* absorption spectrum correspond to the transitions of C 1*s* electrons to the free hybridized states formed from C 2*p* and F 2*p* states. Bands *A* and *B* correspond to the spectra of the initial regions of hexagonal graphene mesh without any fluorine atoms attached. At the same time, no changes are observed in the F 1*s*-spectrum features [Fig. 10(a), curve 3]. These findings become even more evident after the fifth annealing at the temperature $T_{DF}=T_F$=420 °C. Obviously, such changes in C 1*s* and F 1*s* absorption spectra of F-MWCNTs [Figs. 10(a) and 10(b), curve 4] demonstrate the onset of defluorination process, i.e., partial breakage of C-F

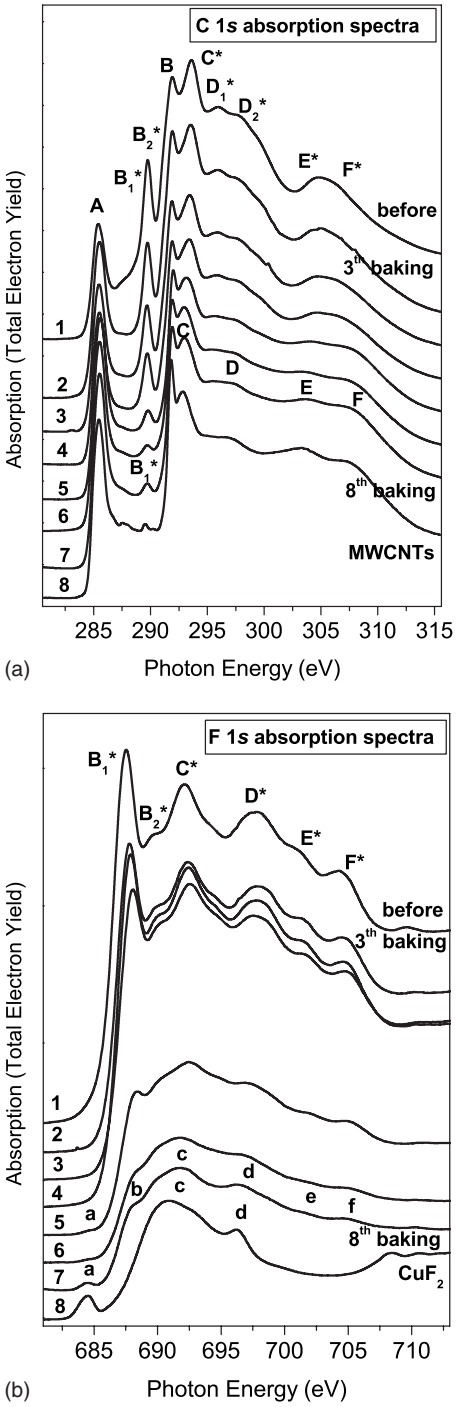

FIG. 10. (a) C 1*s* and (b) F 1*s* absorption spectra of MWCNTs+F39% before and during annealing.

bonds, which, apparently, occurs mainly in the outer layers of F-MWCNTs. After the sixth annealing performed during 15 min at T_{DF}=450 °C, defluorination becomes even more evident, namely, the F 1*s* spectrum begins changing as intensely as the C 1*s* spectrum does [Figs. 10(a) and 10(b), curve 5]. Contrary to the C 1*s* spectrum, the F 1*s* absorption spectrum changes stepwise. The intensities of bands B_1^*-F^* drop instantly, the absorption spectrum as a whole becomes less structured and a weak absorption band *a* emerges in front of the main F 1*s* absorption edge. From the above, it is reasonable to believe that at $T_{DF}=T_F$ intense breakage of earlier formed C-F bonds takes place. What is significant is that the hexagonal carbon mesh is not destructed in this case; this is demonstrated by restoration of the C 1*s* spectrum features typical of the initial MWCNTs and HOPG (π-resonance *A*, σ-resonance *B*, bands *D*, *E*, and *F*). Such restoration of the *A*-*F* bands takes place concurrently with the reduction in bands associated with the transitions of C 1*s* electrons to the hybridized C-F states (bands B_1^*-F^*). Such a behavior of the main spectrum features does not contradict the interpretation of new absorption bands arising in the C 1*s* spectra of F-MWCNTs after fluorination as those reflecting the C 1*s*-electron transition to the hybridized C-F states of the new C-F phase distributed homogeneously through the entire MWCNT depth and formed by attaching fluorine atoms to the carbon-atom $2p_z\pi$ orbitals arranged perpendicular to the graphene layers without destroying the graphene mesh; the new phase manifests itself in corrugating only.

Actually, defluorination of F-MWCNTs is accompanied by modification of the E^*-F^* bands typical of sp^3-hybridized electron states of carbon atoms into the *E* and *F* bands typical of HOPG with sp^2 hybridization of electron states of carbon atoms. After the further 3 hr annealing of the sample under study (carried out in two stages at the same temperature, T_{DF}=450 °C), the C 1*s*-spectrum features reduced after fluorination were restored almost fully [Fig. 10(a), curves 6 and 7], whereas the F 1*s* spectrum varies only slightly [Fig. 10(b), curves 6 and 7]. The most important modification of the latter is a considerable increase in intensity of band *a*. It should be noted that the similar low-energy structures are characteristic of the F 1*s* absorption spectra for 3*d* transition-metal fluorides, and they are caused by transitions of the F 1*s* electrons to low-lying empty electronic states with transition-metal 3*d*—fluorine 2*p*-hybridized character.[51] For the following discussion it is important that a weak isolated band is only observed in the absorption spectrum of copper difluoride CuF_2. Direct comparison between the spectra of defluorinated F-MWCNTs (curve 7) and CuF_2 (curve 8) allows us to state that the spectrum of the former contains in fact a contribution from the F 1*s* spectrum of copper fluoride CuF_x. Clearly the formation of CuF_x on a surface of the copper substrate results from chemical interaction between the copper atoms and the fluorine ones that are derived from the thermal defluorination of F-MWCNTs. This assumption is in good agreement with an appearance of 2*p*-3*d* resonance in Cu 2*p* absorption spectrum of F-MWCNTs on the copper substrate; this resonance is lacking in the spectrum of the copper metal. These findings testify that separate fluorine atoms are mainly detached during the thermal defluorination of F-MWCNTs. The identity of C 1*s* absorption spectra of defluorinated MWCNTs+F39% and MWCNTs also demonstrate the absence of any remarkable amorphous component in the sample after annealing the sample. Therefore, the experiment performed makes it possible to affirm that thermal annealing of F-MWCNTs allows their defluorination almost free of destruction of the hexagonal graphene mesh.

In this work we used MWCNTs of the "Russian doll" type produced by the electric-arc method. At present it is generally recognized that those tubes are characterized by maximally perfect graphene sheets forming the tube lateral

walls.[52,53] The procedure initial MWCNT cleaning and subsequent fluorination were developed so as to prevent mass opening of MWCNT internal channels. The fact that the tube channels are closed was confirmed by HRTEM measurements. We have found out that the MWCNT defectiveness was about 10%. Those initial MWCNT defects promoted fluorine penetration inside MWCNTs in the process of fluorination and fluorine removal from MWCNTs in the process of defluorination. In addition, the fluorination itself gives rise to insignificant number of defects, which is confirmed by other researchers.[31,54]

The initial MWCNT properties are similar to those of graphite (see, e.g., Ref. 1). Thus we assume that the fluorination process may be similar to that in graphite,[8,55] and we have shown that when a fluorine atom is placed above near the center of hexagon, the optimal position of the fluorine atom is not above the center of a hexagonal ring of carbon atoms, as is commonly observed in alkali-metal-doped graphicte intercalated compounds (GICs) but above one of six central carbon atoms (under the assumption that a covalent C-F bond is formed). A local deformation of the carbon skeleton is observed, which is the evidence of carbon-atom rehybridization from sp^2 to sp^3.

IV. CONCLUSIONS

The combined investigation of the fluorinated MWCNTs by highly chemically sensitive x-ray methods (NEXAFS and XPS) is presented. The formation of the C-F covalent bond similar to the one in WGF in the F-MWCNT is observed. The NEXAFS measurements on the C 1*s* and F 1*s* absorption edges of the F-MWCNTs and reference compounds demonstrated that within the probing depth (~15 nm) of the carbon nanotubes, the process of fluorination occurs uniformly and does not depend on the fluorine concentration. The interaction of fluorine atoms with MWCNTs proceeds through the covalent attachment of fluorine atoms to graphene layers of the graphite skeleton without its destruction and is accompanied by a change in the hybridization of the 2*s* and 2*p* valence electron states of the carbon atom from the trigonal (sp^2) to tetrahedral (sp^3) hybridization. The very surface-sensitive XPS measurements indicate the presence of the additional C-F phase at the surface of the F-MWCNTs. Based on the above-described information we conclude that the C-F bond formation is nearly homogeneous through the tubes; we observed the same type of bond at the surface and in the bulk of the material, except the very surface region.

ACKNOWLEDGMENTS

This work was performed within the framework of the "Russian-German Laboratory at BESSY" bilateral Program and supported by the Russian Foundation for Basic Research (Projects No. 06-02-16998 and No. 09-02-01278) and the International Association of Assistance for the Promotion of Cooperation with Scientists from the New Independent States of the Former Soviet Union (Project INTAS No. 04-80-6932). We would like to thank L. Makhova (Universität Leipzig) for help during experiments and Yu. M. Shulga (Institute of Problems of Chemical Physics, RAS) for helpful discussion.

*Corresponding author. ALBA-CELLS, Carretera BP 1413, de Cerdanyola del Vallès a Sant Cugat del Vallès, Km. 3,3, 08290 Cerdanyola del Vallès (Barcelona), Spain; mbrzhezinskaya@cells.es

[1] M. S. Dresselhaus, G. Dresselhaus, and P. Avouris, *Carbon Nanotubes: Synthesis, Structure, Properties and Applications: Topics in Applied Physics* (Springer-Verlag, Berlin, 2001), Vol. 80.
[2] M. Burghard, Surf. Sci. Rep. **58**, 1 (2005).
[3] J. L. Bahr and M. J. Tour, J. Mater. Chem. **12**, 1952 (2002).
[4] E. T. Mickelson, C. B. Huffman, A. G. Rinzler, R. E. Smalley, R. H. Hauge, and J. L. Margrave, Chem. Phys. Lett. **296**, 188 (1998).
[5] E. T. Mickelson, I. W. Chiang, J. L. Zimmerman, P. J. Boul, J. Lozano, J. Liu, R. F. Smalley, R. H. Hauge, and J. L. Margrave, J. Phys. Chem. B **103**, 4318 (1999).
[6] V. N. Khabashesku, W. E. Billups, and J. L. Margrave, Acc. Chem. Res. **35**, 1087 (2002).
[7] Y.-S. Lee, J. Fluorine Chem. **128**, 392 (2007).
[8] H. Touhara and F. Okino, Carbon **38**, 241 (2000).
[9] A. Hamwi, H. Alvergnat, S. Bonnamy, and F. Béguin, Carbon **35**, 723 (1997).
[10] N. F. Yudanov, A. V. Okotrub, Yu. V. Shubin, L. I. Yudanova, L. G. Bulusheva, A. L. Chuvilin, and J.-M. Bonard, Chem. Mater. **14**, 1472 (2002).
[11] T. Hayashi, M. Terrones, C. Scheu, Y. A. Kim, M. Rühle, T. Nakajima, and M. Endo, Nano Lett. **2**, 491 (2002).
[12] Y. S. Lee, T. H. Cho, B. K. Lee, J. S. Rho, K. H. An, and Y. H. Lee, J. Fluorine Chem. **120**, 99 (2003).
[13] K. H. An, J. G. Heo, K. G. Jeon, D. J. Bae, C. Jo, C. W. Yang, C.-Y. Park, Y. H. Lee, Y. S. Lee, and Y. S. Chung, Appl. Phys. Lett. **80**, 4235 (2002).
[14] K. N. Kudin, H. F. Bettinger, and G. E. Scuseria, Phys. Rev. B **63**, 045413 (2001).
[15] K. A. Park, Y. S. Choi, Y. H. Lee, and C. Kim, Phys. Rev. B **68**, 045429 (2003).
[16] N. G. Lebedev, I. V. Zaporotskova, and L. A. Chernozatonskii, Microelectron. Eng. **69**, 511 (2003).
[17] G. Van Lier, C. P. Ewels, F. Zuliani, A. De Vita, and J.-C. Charlier, J. Phys. Chem. B **109**, 6153 (2005).
[18] C. P. Ewels, G. Van Lier, J. C. Charlier, M. I. Heggie, and P. R. Briddon, Phys. Rev. Lett. **96**, 216103 (2006).
[19] J. Stöhr, *NEXAFS Spectroscopy*, Springer Series in Surface Science Vol. 25 (Springer-Verlag, Berlin, 1992).
[20] J. G. Chen, Surf. Sci. Rep. **30**, 1 (1997).
[21] A. Kuznetsova, I. Popova, J. T. Yates, Jr., M. J. Bronikowski, C. B. Huffman, J. Liu, R. E. Smalley, H. H. Hwu, and J. G. Chen, J. Am. Chem. Soc. **123**, 10699 (2001).
[22] Y. H. Tang, T. K. Sham, Y. F. Hu, C. S. Lee, and S. T. Lee,

Chem. Phys. Lett. **366**, 636 (2002).
[23] J. Schiessling, L. Kjeldgaard, F. Rohmund, L. K. L. Falk, E. E. B. Campbell, J. Nordgren, and P. A. Brühwiler, J. Phys.: Condens. Matter **15**, 6563 (2003).
[24] S. Banerjee, T. Hemraj-Benny, M. Balasubramanian, D. A. Fisher, J. A. Misewich, and S. S. Wong, Chem. Commun. (Cambridge) **2004**, 772.
[25] S. Banerjee, T. Hemraj-Benny, S. Sambasivan, D. A. Fischer, J. A. Misewich, and S. S. Wong, J. Phys. Chem. B **109**, 8489 (2005).
[26] T. Hemraj-Benny, S. Banerjee, S. Sambasivan, D. A. Fischer, G. Eres, A. A. Puretzky, D. B. Geohegan, D. H. Lowndes, J. A. Misewich, and S. S. Wong, Phys. Chem. Chem. Phys. **8**, 5038 (2006).
[27] J. Zhou, X. Zhou, X. Sun, R. Li, M. Murphy, Z. Ding, X. Sun, and T.-K. Sham, Chem. Phys. Lett. **437**, 229 (2007).
[28] A. P. Lukirskiy and I. A. Brytov, Fiz. Tverd. Tela (Leningrad) **6**, 43 (1964) [Sov. Phys. Solid State **6**, 32 (1964)].
[29] W. Gudat and C. Kunz, Phys. Rev. Lett. **29**, 169 (1972).
[30] S. Huefner, *Photoelectron Spectroscopy* (Springer, Berlin, 1996).
[31] A. V. Okotrub, N. F. Yudanov, A. L. Chuvilin, I. P. Asanov, Yu. V. Shubin, L. G. Bulusheva, A. V. Gusel'nikov, and I. S. Fyodorov, Chem. Phys. Lett. **322**, 231 (2000).
[32] Y. M. Shulga, T.-C. Tien, C.-C. Huang, S.-C. Lo, V. E. Muradyan, N. V. Polyakova, Y.-C. Ling, R. O. Loufty, and A. P. Moravsky, J. Electron Spectrosc. Relat. Phenom. **160**, 22 (2007).
[33] M. M. Brzhezinskaya, N. A. Vinogradov, V. E. Muradyan, Yu. M. Shulga, N. V. Polyakova, and A. S. Vinogradov, Fiz. Tverd. Tela (St. Petersburg) **50**, 565 (2008) [Phys. Solid State **50**, 587 (2008)].
[34] M. M. Brzhezinskaya, N. A. Vinogradov, V. E. Muradyan, Yu. M. Shulga, R. Puettner, A. S. Vinogradov, and W. Gudat, Phys. Solid State (to be published).
[35] Yu. M. Shul'ga, I. A. Domashnev, B. P. Tarasov, A. M. Kolesnikova, E. P. Krinichnaya, V. E. Muradyan, and N. Yu. Shul'ga, Altern. Energ. Ekol. **1**, 70 (2002).
[36] N. A. Kiselev, A. P. Moravsky, A. B. Ormont, and D. N. Zakharov, Carbon **37**, 1093 (1999).
[37] S. L. Molodtsov, S. I. Fedoseenko, D. V. Vyalikh, I. E. Iossifov, R. Follath, S. A. Gorovikov, M. M. Brzhezinskaya, Yu. S. Dedkov, R. Puettner, J.-S. Schmidt, V. K. Adamchuk, W. Gudat, and G. Kaindl, Appl. Phys. A: Mater. Sci. Process. **94**, 501 (2009).
[38] A. S. Vinogradov, A. Yu. Dukhnyakov, V. M. Ipatov, D. E. Onopko, A. A. Pavlychev, and S. A. Titov, Fiz. Tverd. Tela (Leningrad) **24**, 1417 (1982) [Sov. Phys. Solid State **24**, 803 (1982)].
[39] P. A. Brühwiler, A. J. Maxwell, C. Puglia, A. Nilsson, S. Andersson, and N. Mårtensson, Phys. Rev. Lett. **74**, 614 (1995).
[40] R. Nyholm, S. Svensson, J. Nordgren, and A. Flodstrom, Nucl. Instrum. Methods Phys. Res. A **246**, 267 (1986).
[41] P. E. Batson, Phys. Rev. B **48**, 2608 (1993).
[42] G. Comelli, J. Stöhr, C. J. Robinson, and W. Jark, Phys. Rev. B **38**, 7511 (1988).
[43] Yu. M. Shul'ga, V. E. Muradyan, V. M. Martynenko, B. P. Tarasov, and N. V. Polyakova, Fullerenes, Nanotubes, Carbon Nanostruct. **14**, 243 (2006).
[44] R. A. Rosenberg, P. J. Love, and V. Rehn, Phys. Rev. B **33**, 4034 (1986).
[45] A. P. Hitchcock, P. Fischer, A. Gedanken, and B. Robin, J. Phys. Chem. **91**, 531 (1987).
[46] V. Gupta, T. Nakajima, Y. Ohzawa, and B. Zemva, J. Fluorine Chem. **120**, 143 (2003).
[47] Y. Sato, R. Hagiwara, and Y. Ito, Solid State Sci. **5**, 1285 (2003).
[48] M. M. Brzhezinskaya and E. M. Baitinger, *Trends in Carbon Nanotube Research* (Nova Science, New York, 2005), pp. 235–275.
[49] F. C. Brown, R. Y. Bachrach, and A. Bianconi, Chem. Phys. Lett. **54**, 425 (1978).
[50] C. Martin, E. T. Arakawa, T. A. Callcott, and J. C. Ashley, J. Electron Spectrosc. Relat. Phenom. **35**, 307 (1985).
[51] A. S. Vinogradov, S. I. Fedoseenko, S. A. Krasnikov, A. B. Preobrajenski, V. N. Sivkov, D. V. Vyalikh, S. L. Molodtsov, V. K. Adamchuk, C. Laubschat, and G. Kaindl, Phys. Rev. B **71**, 045127 (2005).
[52] B. Lukic, J. W. Seo, R. R. Bacsa, S. Delpeux, F. Beguin, G. Bister, A. Fonseca, J. B. Nagy, A. Kis, S. Jeney, A. J. Kultik, and L. Forro, Nano Lett. **5**, 2074 (2005).
[53] J.-P. Salvetat, A. J. Kulik, J.-M. Bonard, G. A. D. Briggs, T. Stockli, S. Bonnamy, F. Beguin, N. A. Burnham, and L. Forro, Adv. Mater. (Weinheim, Ger.) **11**, 161 (1999).
[54] O. Zhou, R. M. Fleming, D. W. Murphy, C. H. Chen, R. C. Haddon, A. P. Ramirez, and S. H. Glarum, Science **263**, 1744 (1994).
[55] R. Saito, M. Yagi, T. Kimura, G. Dresselhaus, and M. S. Dresselhaus, J. Phys. Chem. Solids **60**, 715 (1999).